Confinement Properties of Small Aspect Ratio Tokamak/Stellarator Hybrid Devices

D. A. Spong, S. P. Hirshman, J. C. Whitson
Oak Ridge National Laboratory

[to be submitted to the journal Plasma Physics Reports issue with the collection of papers from 1996 US-Japan JIFT Stellarator Workshop, Columbia University]

Abstract

We have examined the confinement properties for a range of small aspect ratio tokamak/stellarator hybrid devices. Vacuum rotational transform is produced in these configurations using relatively simple tilted/modulated toroidal magnetic field coils which can then be supplemented with driven plasma current. The iota profile is tokamak-like with a maximum in the center and decreasing towards the plasma edge. Evaluation of confinement characteristics is carried out on several levels including: B_{min}, B_{max} contours, longitudinal adiabatic invariant J* contours, guiding-center trajectories, and Monte Carlo simulations starting with a random ensemble of particles. We find that confinement generally improves with increasing driven current, lower ripple, increasing magnetic field, and increasing electric field. Another avenue for confinement improvement is through optimization of the magnetic geometry. The tools mentioned above for evaluating confinement suggest several simple criteria as targets for the magnetic optimizations.

I. Introduction

Existing stellarators have typically been designed at large aspect ratio and in such a way as to minimize the amount of plasma current. However, the economics of fusion power systems place a premium on compactness. There has recently been interest[1,2,3,4,5,6] in the possibility that tokamak/stellarator hybrid devices which combine tokamak-like driven current with vacuum stellarator transform could allow better access to the low aspect ratio stellarator design space in a manner which would combine the best features of both devices. Relative to the tokamak, these systems would offer: less disruption potential, eased requirements for non-inductive startup, and steady-state operation. Relative to the pure stellarator they would offer: larger volume flux surfaces, lower aspect ratio, the possibility of more robust flux surfaces at high plasma β, and a tokamak-like iota profile which decreases towards the plasma edge. The latter feature can have several important implications: a more toroidally symmetric divertor separatrix and an absence of large islands near the plasma edge (due to the higher order of the resonances as iota decreases). In Figure 1 we show 3D visualizations of the outer flux surfaces and filamentary coils for the 2, 4, and 8 field period versions of the hybrid devices which we shall examine in this paper.

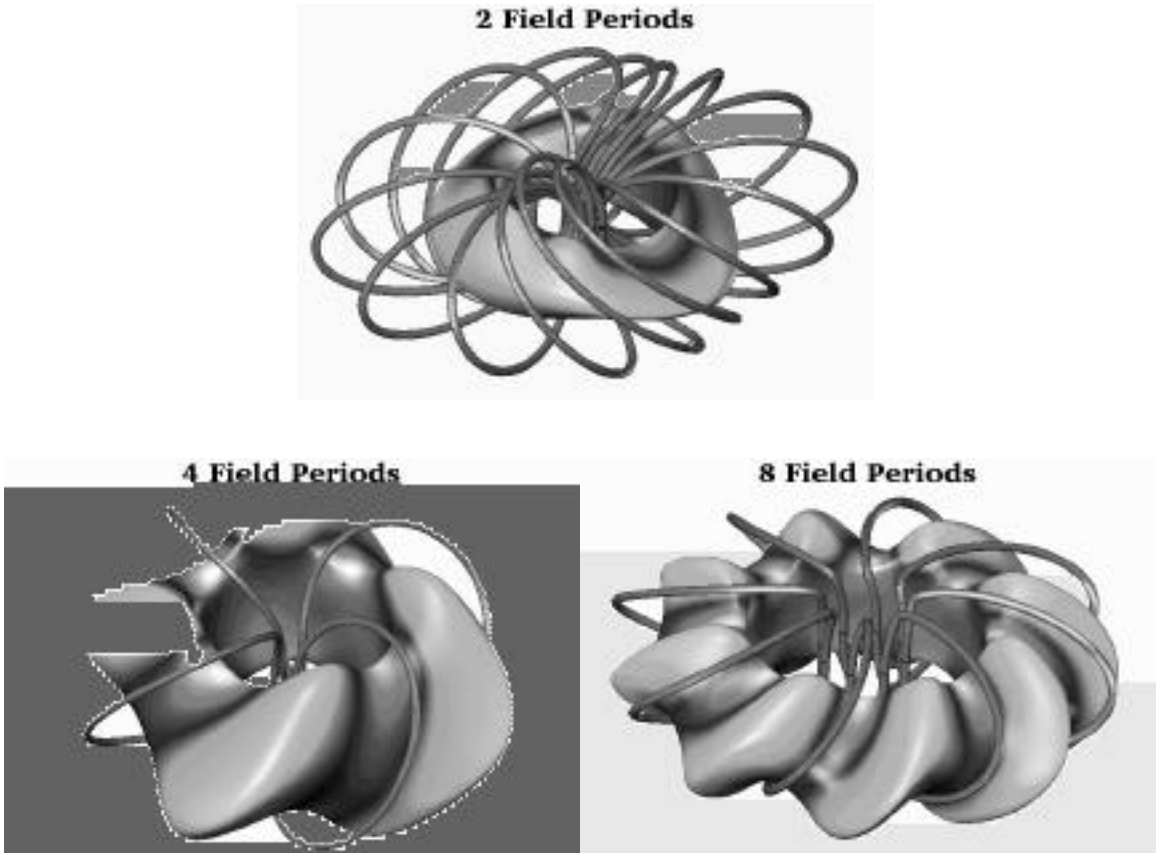

Figure 1 - Typical coil configurations and outermost flux surfaces for 2, 4, and 8 field period low aspect ratio tokamak/stellarator hybrid devices.

Particle confinement and transport is a significant issue for these devices. The provision of vacuum rotational transform with relatively few coils at low aspect ratio invariably leads to large magnetic field ripple and the associated $1/\nu$ transport regimes. The low aspect ratio (relative to conventional stellarators) results in stronger toroidal field ripple and larger orbit displacements from flux surfaces. One can therefore expect that some degree of optimization will be required for these devices. It has been shown[7] that the quasi-helical optimization approach can only be achieved to third order in an inverse aspect ratio expansion, thus implying its inapplicability at very low aspect ratios. For these reasons, we expect different optimization strategies than quasihelical symmetrization will be of interest at low aspect ratio. Our goals are first to characterize the levels of transport present in these devices, next to find out what dependencies they have on parameters such as ambipolar electric fields, toroidal plasma current, collisionality, plasma β, and magnetic configuration. The work presented here is in the nature of a progress report as we have primarily analyzed non-optimized configurations. New approaches for the optimization of low aspect ratio devices have recently been suggested[8,9] and application of such techniques is currently in progress. In addition, the confinement evaluation tools we discuss are in a continuing state of improvement.

We shall begin by describing several simple measures of particle confinement quality (B_{min}, B_{max}, J^*) which can be evaluated relatively quickly. These measures will later be useful for

optimization criteria. Next, we describe Monte Carlo transport calculations which have been carried out for ion transport for a range of different low aspect ratio configurations. In addition to the standard non-optimized configurations, we also apply these measures to several recently obtained optimized systems.

II. Bounce-Averaged Projections of Particle Orbits

We first discuss analysis of particle orbits in 3D stellarator equilibria using bounce-averaged methods since they are more rapid to evaluate and reduce the available parameter space to a more manageable level than following the full guiding center orbit trajectories. The following calculations are based on 3D stellarator equilibria which have been transformed into Boozer magnetic coordinates. We have used the VMEC[10] stellarator equilibrium code coupled with a vacuum magnetic field code (AVAC) which calculates the fields produced by the discrete coils using a Green's function approach. Free-boundary, finite β equilibria are found to exist for all of the configurations shown in Figure 1. Transformation to Boozer coordinates[11] is then carried out by equating the contravariant representations of the magnetic field in both coordinate systems. This leads to a field-line differential equation for a doubly-periodic angle transformation function. Singularities in this equation at rational surfaces are then resolved by factoring B^2 into co- and contravariant components. We find that maintenance of adequate convergence in the Boozer space representation of B can require 400 to 600 Fourier modes for low aspect ratio devices

The longitudinal bounce invariant $J = \int m v_{||} dl$ provides an efficient way to evaluate confinement of stellarator orbits. Its validity is based on the assumption that an orbit does not drift a significant amount during a bounce. Since the bounce frequency scales as $E^{1/2}$ (E = energy) and the cross-field drifts scale as E, there will generally be some upper limit in energy beyond which J breaks down. However, for orbits at typical thermal energies in moderately high field period devices, this energy is generally high enough not to pose a limitation. In order to then readily analyze a full range of pitch angles, a further simplification of J is necessary. It has been shown[12] that J may be approximated by a reduced form, denoted by J*, in which the integration along the field line is replaced by an integration over the Boozer toroidal angle coordinate (over a single field period); this is generally valid if the rotational transform per field period is small ($\iota/N << 1$). More precise criteria for the validity of J* have been given in Ref. 12. The motivation for the use of J* is that it simplifies the categorization of orbits into three classes[13]: trapped, trapped/passing transitional, and passing. If the full bounce invariant, J, were used, more classes of trapped orbits would need to be delineated, depending on whether their bounce motion encompassed one field period, two field periods, etc.

A typical set of J* contours for an 8-field period tokamak/stellarator hybrid device is shown in Figure 2. Here we have kept the energy fixed at 1000 ev, included a radially varying electrostatic potential which reaches $e\varphi/kT_{ion} = 0.7$ at the edge, and varied the ratio of the energy to the magnetic moment (ε/μ), which is our pitch angle-like variable.

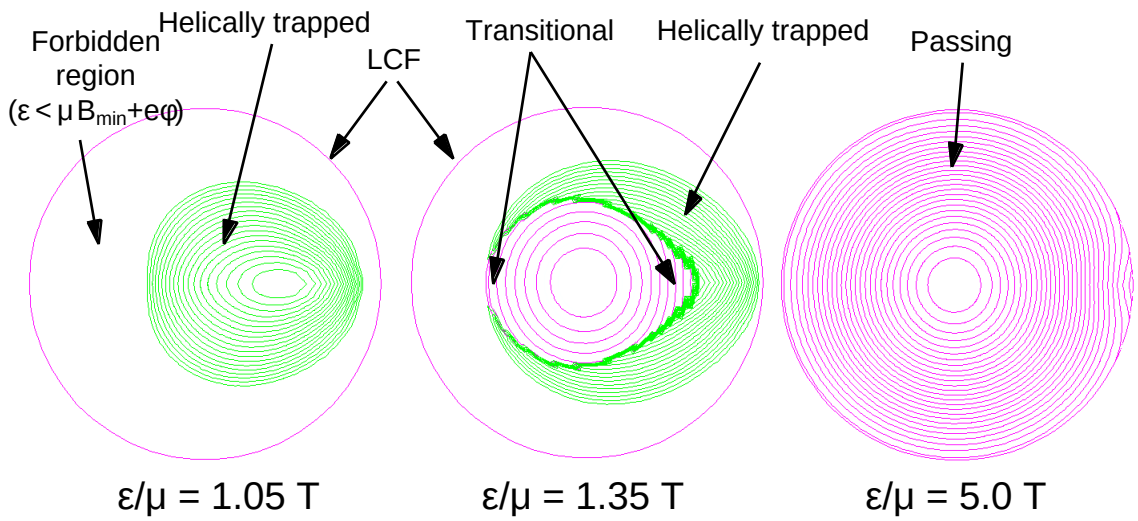

Figure 2 - J* contours showing transition from helically trapped to passing orbits

Cases are shown with (a) only trapped J* contours, (b) passing, transitional and trapped contours, and (c) only passing contours. The contours of J* (approximate orbit trajectories) are plotted in a poloidal plane in Boozer space (flux surfaces are concentric circles). It is important to note that in using a constant-of-motion parameter such as ε/μ, positive values of $v_{||}^2 = \varepsilon - \mu B - e\varphi$ will not necessarily exist for arbitrarily specified points in the cross-section.[13] These are denoted as forbidden regions and indicated by blank regions without contour lines in our figures. The topology of the boundaries between forbidden, trapped, transitional, and passing J* contours can be expressed in terms of the B_{min}, and B_{max} functions. These are defined respectively as the minimum and maximum values of B as one moves in Boozer coordinates along toroidal angle φ at constant ψ and θ. The boundaries between the various types of orbits can be written as:

$$0 < (\varepsilon/\mu)(1 - q\varphi/\varepsilon) < B_{min} \qquad \text{forbidden region}$$

$$B_{min} < (\varepsilon/\mu)(1 - q\varphi/\varepsilon) < B_{max} \qquad \text{helically trapped orbits} \qquad (1)$$

$$B_{max} < (\varepsilon/\mu)(1 - q\varphi/\varepsilon) \qquad \text{mixture of transitional and passing orbits}$$

The contour $B_{min} = (\varepsilon/\mu)(1 - q\varphi/\varepsilon)$ then separates the forbidden and helically trapped regions while the contour $B_{max} = (\varepsilon/\mu)(1 - q\varphi/\varepsilon)$ forms the boundary between helically trapped and passing/transitional orbits. B_{min} contours are also useful as approximations to the trajectories of deeply trapped orbits in the absence of an electric field. In Figure 3 we compare B_{min} contours with J* contours for deeply trapped ions without an electric field (all of which are unconfined here) and B_{max} contours with a set of J* contours which have a boundary between helically passing and trapped/transitional orbits.

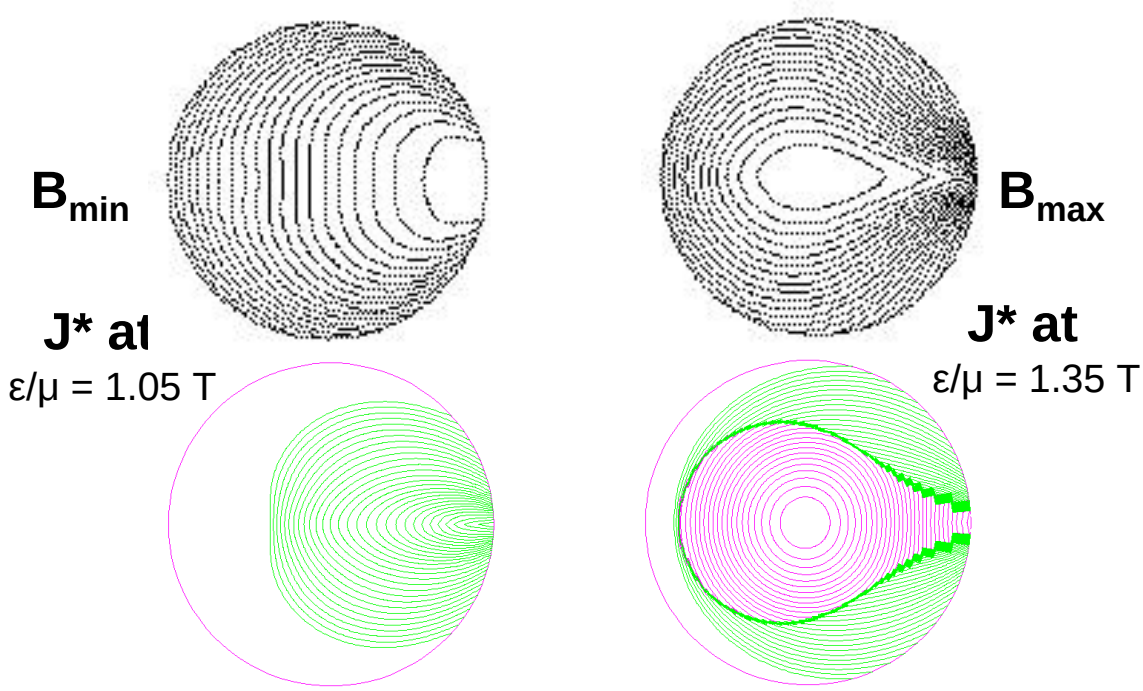

Figure 3 - Comparison of B_{min} contours with deeply trapped J* contours (left) and B_{max} contours with trapped/transitional J* contours (right).

As may be seen, the B_{min} contours roughly follow the deeply trapped J* contours. As will be discussed further in section IV, the centering of B_{min} contours on flux surfaces can be a useful optimization criteria for the confinement of trapped orbits. The B_{max} contours align with the boundary between passing/transitional orbits and purely helically trapped orbits. Making B_{max} constant on a flux surface can lead to a reduction of transitional orbits. This comes from the fact that in order to be transitional, a J* contour must intersect the B_{max} contour at a finite grazing angle; otherwise it would close on itself and become a passing orbit. Since the passing J* contours are nearly centered circles, making the B_{max} contours also centered circles would leave no room for transitional orbits to fit in between the B_{max} contours and outermost passing orbits. For this reason, our optimization approach will also attempt to center the B_{max} contours on flux surfaces.

We have also adapted a guiding center symplectic orbit trajectory code[13,14] to our low aspect ratio hybrid devices. This code integrates the coupled Hamiltonian equations[11] for $d\theta/dt$, $d\varphi/dt$, dP_θ/dt, and dP_φ/dt in time in such a way as to approximately conserve the total energy. These trajectories have been overlaid on a set of J* contours based on the same value of energy and ε/μ as the orbit. Such comparison plots are shown in Figure 4 for 1 keV helically trapped, transitional and passing ions with no electric field present.

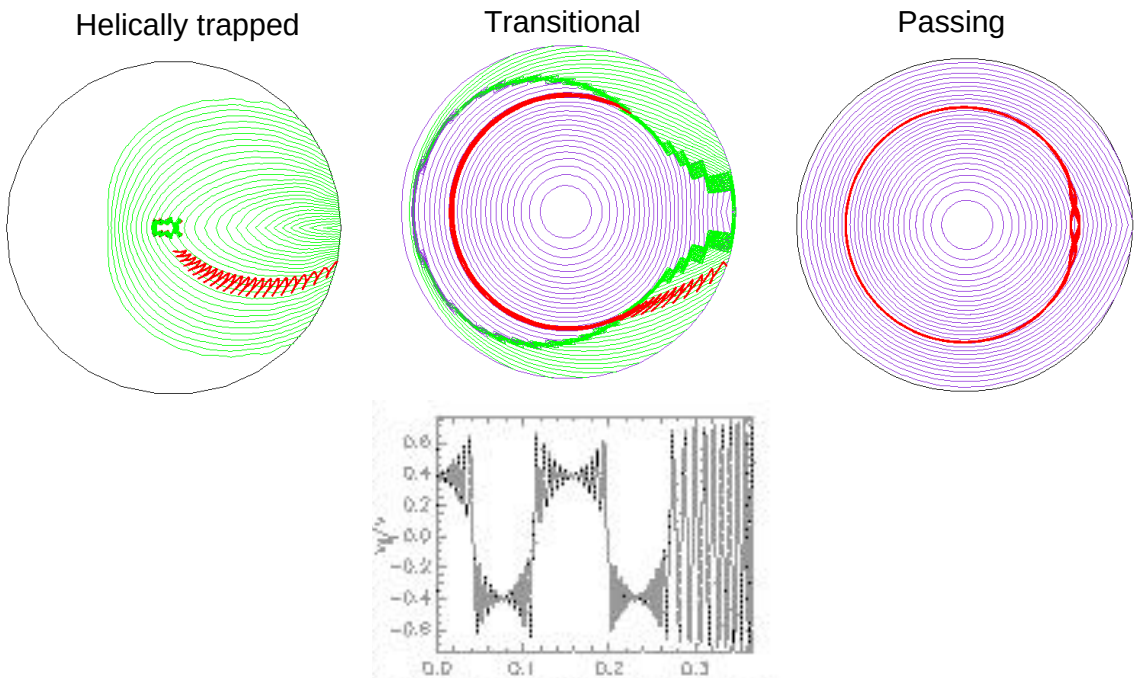

Figure 4 - Comparison of particle guiding center trajectories with associated J* contours

As may be seen, on the average, orbit trajectories follow J* contours. For the transitional orbit we have also shown the time dependence of the ratio of the parallel velocity to the total velocity ($v_{||}/v$). From J* itself we cannot predict at what point the orbit will change from passing to helically trapped. This depends on the relative alignment between the orbit's bounce phase and the helical field ripple. Methods for calculating such transition probabilities without solving the full orbit trajectory equations have been discussed in.Ref. 12 We generally find good agreement as shown in Figure 4 between J* contours and orbit trajectories, except for certain classes of transitional orbits which are in the vicinity of the separatrix locations[15].

J* surfaces then provide a relatively quick way of assessing confinement in low aspect ratio devices. The location of these contours depends on the parameters of energy, ε/μ, and electric field. For trapped orbits without an electric field, there is no dependence on energy. In order to encompass all types of orbits, ε/μ typically should be varied from $B_{min,\ global}$ up to $B_{max,\ global}$ (i.e., the minimum/maximum in B over the whole volume). For $\varepsilon/\mu > B_{max,\ global}$ most of the volume is occupied by passing particles. For the low aspect ratio devices examined here, the helically trapped orbits have the poorest confinement so we have focused most of our attention on mechanisms for closing and centering their J* contours. Electric fields provide one avenue for improving trapped orbits. In Figure 5 such effects are shown.

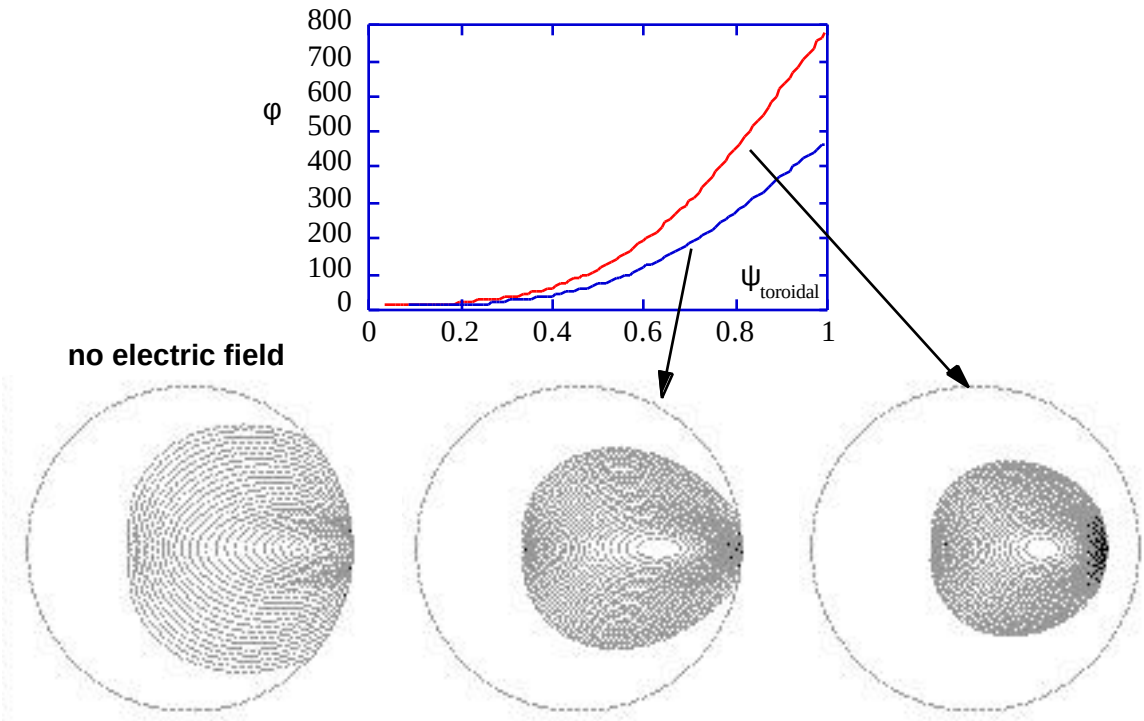

Figure 5 - Effect of electric field on ion J* contours.

The above plots have been made for 1000 ev ion orbits. In Figure 6 we show typical J* contours for 1000 ev electrons in an 8 field period device at varying levels of electric field. In contrast to the ion orbits at $\varepsilon/\mu = 1.05$, the electron J* contours show a mixture of trapped, passing, and transitional orbits and the helically trapped orbits for $e\varphi_0/kT_e > 1$ now occur inside the region of the passing orbits. As the electric field is increased, the electron confinement also improves and by $e\varphi_0/kT_e = 2$ all orbits for this case ($\varepsilon/\mu = 1.05$, $T_e = 1000$ ev) are also confined.

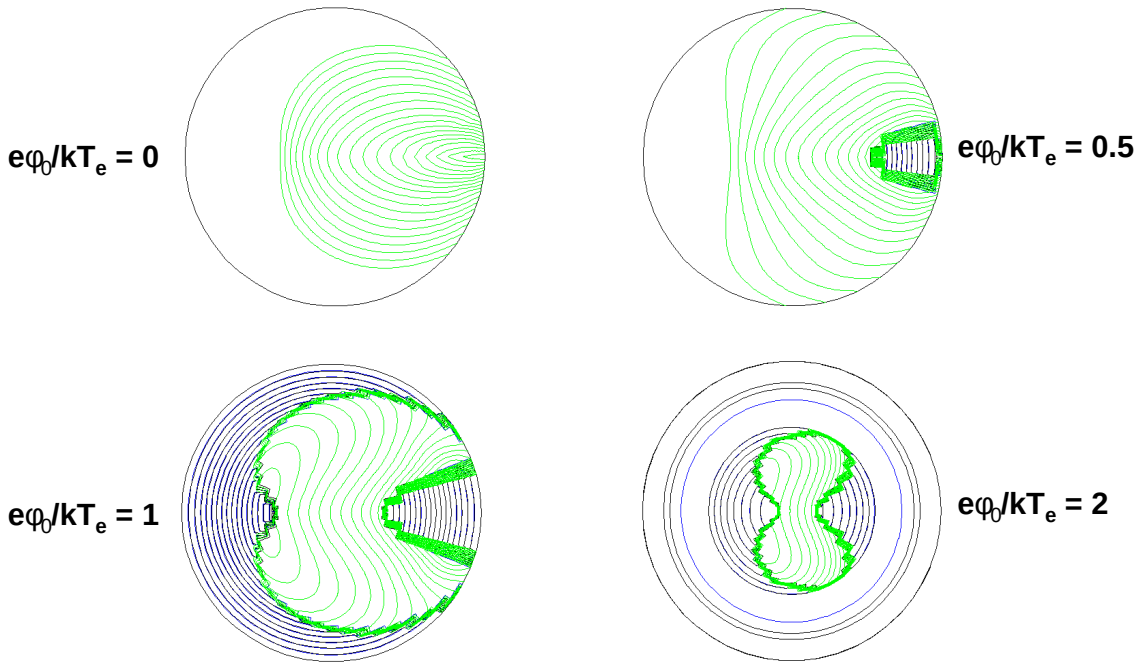

Figure 6 - Dependence of electron J* contours on the electric field

III. Monte Carlo Transport Simulations

In the preceding section, several measures of single particle confinement in hybrid systems were discussed. Although these are useful for indicating regions of configuration and velocity space where direct orbit losses may occur, they do not provide information on the rate of these losses, nor do they indicate the level of the slower, diffusive losses. Monte Carlo methods.[16,17,18,19] have been used extensively to evaluate both diffusive and direct particle losses in stellarators. This approach is well suited for configurations which require a large spectrum of Fourier modes to represent the equilibrium B field and configurations with classes of orbits that have large displacements from flux surfaces. An alternative approach being developed is direct solution of the drift kinetic equation using variational techniques.[20] The advantage of this method is that it provides the full transport matrix, but it is still inherently a diffusive model and cannot evaluate the direct particle losses.

We have adapted an earlier Monte Carlo model[16] to our configurations. This model launches an ensemble of particles on a single interior flux surface, randomly distributed in pitch angle, and in toroidal and poloidal angles. The particle energies are chosen in such a way as to approximate a Maxwellian distribution. The orbits of these particles are then followed using the Hamiltonian guiding center equations and with the B field calculated based on the full set of equilibrium B_{mn} Fourier modes. We have found that improvements in the efficiency of the code can be obtained by initially fitting the ψ, θ, and φ dependencies of B with 3D splines. Although this leads to some loss of accuracy, it has not proven significant for the cases we have benchmarked. As the particles leave the outermost flux surface, they are restarted at the initial flux surface in order to conserve particle number density. An alternate approach where the particles are removed from the distribution as they are lost is also being implemented; in this case, particle and energy lifetimes could be inferred by observing decay rates.

In Figure 7 rotational transform profiles and B(φ) on the magnetic axis are plotted for a number of the cases which we have analyzed. Our typical test case takes T_{ion} = 1000ev, n_{ion} = 10^{13} cm^{-3}, with constant (flat) profiles for the background ion density and temperature. The test ions (also at 1000 ev) are started out at ψ/ψ_{edge} = 0.25 (ψ = toroidal flux).

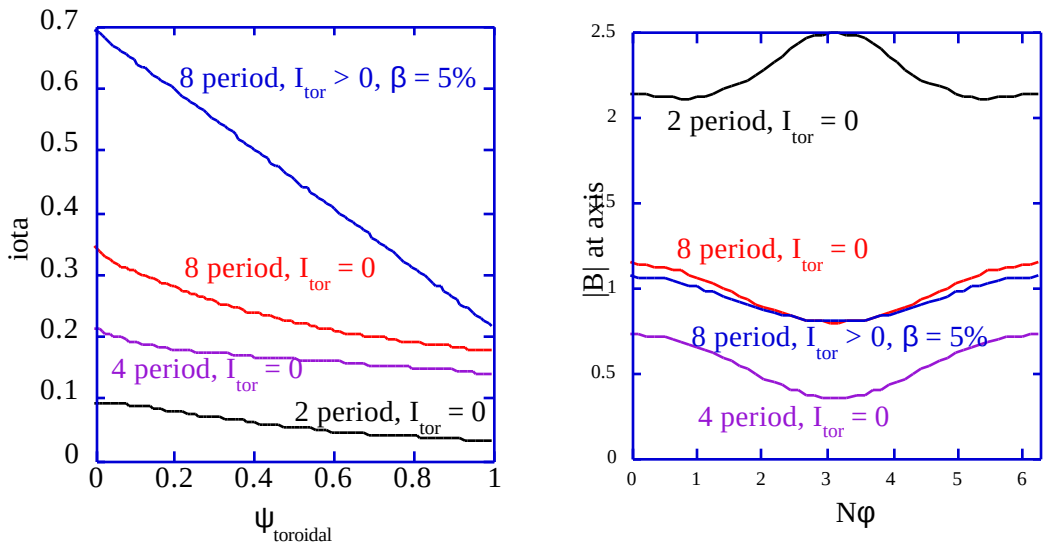

Figure 7 - Iota profiles and variation of |B| vs. toroidal angle (over one field period)

These parameters result in low collisionality relative to drift times and tend to emphasize direct losses (when they are present). For this reason, in the following we will present only the global particle and energy loss rates through the outermost flux surface and will not discuss local diffusive loss rates. More recent calculations with higher densities and lower temperatures have shown that regimes are possible in these devices where diffusive losses dominate. We have tried cases with 256 to 1024 particles (currently limited by computational time) and not found significant differences; most of the results presented here are based on 256 particles. Of course, due to the continual replacement of particles passing through the last closed flux surface, the net particles followed over the course of a calculation will be greater than these numbers. We typically try to follow the test particle distribution for 2 to 4 collision times. Particle and energy loss rates vs. time for the cases shown in Figure 7 are plotted in Figure 8.

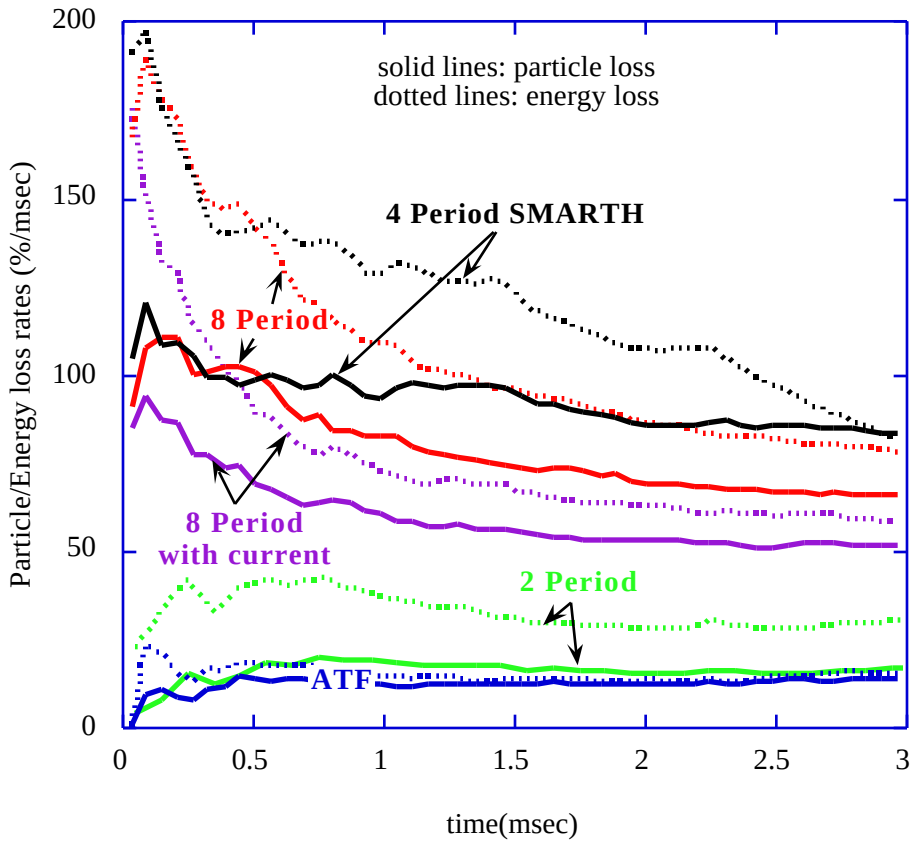

Figure 8 - Monte Carlo particle and energy loss rates vs. time for cases of Figure 7.

We have chosen to normalize the loss rates (shown here as percent per millisecond) to the number of particles launched initially. Due to the above mentioned continual replacement of lost orbits, the total number of particles followed throughout the calculation will generally exceed this number; one could also consider normalizing to this latter number which would tend to bring the above curves closer together. The 4 period device has the highest loss rates due to its lower magnetic field and high relative ripple. The 2 period device shows the lowest loss rates as a result of its lower ripple and is approaching ATF[21] levels of transport. The indication of ≈ 10% per msec loss rates for ATF is consistent with its observed confinement times. The 8 period device is in between and shows that net toroidal current (at a level which roughly doubles iota) leads to about a 25% reduction in loss rates. As may be seen, the devices with higher loss rates typically show a peaking of the loss at early times in the calculation. This is likely attributed to the fact that direct particle losses are largest at early times; as time progresses, particle replacement of the orbits passing through the last closed flux surface will tend to select out a subpopulation of

orbits which are better confined. Since we are primarily interested in relative comparisons between the different configurations here, we have not attempted to correct for this effect.

In Figure 9 we show the dependence of particle and energy loss rates on the electric field for the 8 field period device with current. As may be seen, increasing values of potential lead to a secular reduction in the particle and energy loss rates.

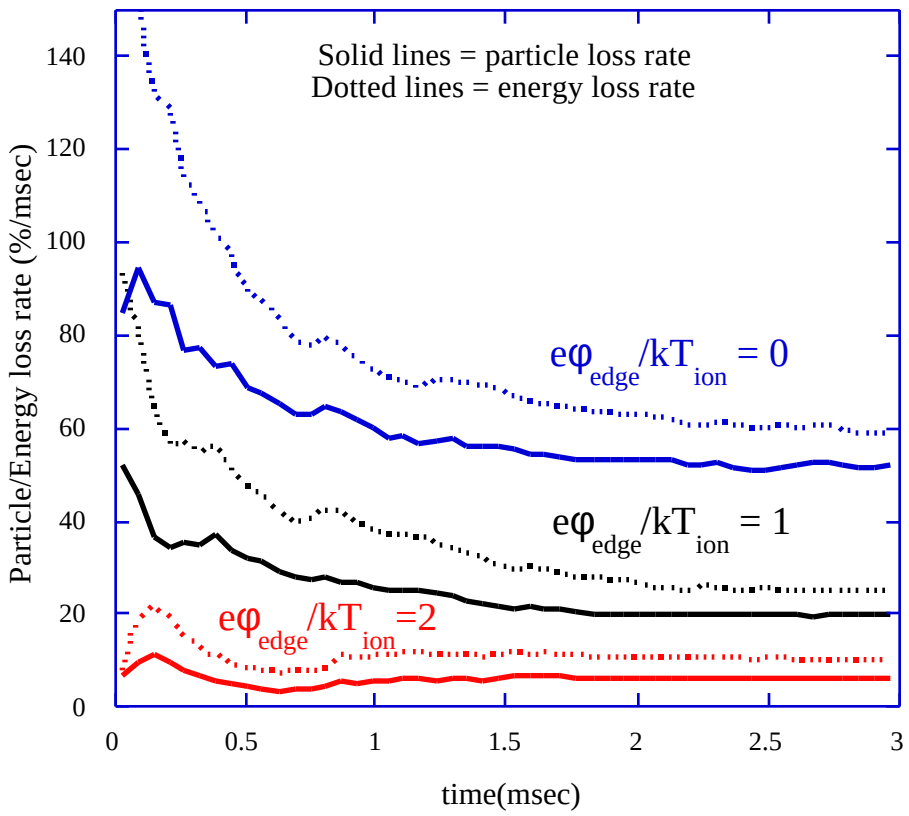

Figure 9 - Monte Carlo particle and energy loss rates vs. time for several values of electric field.

In Figure 10 plots are given of projections of the particle trajectory cloud on a fixed poloidal plane along with trapped J* contours for cases from Figure 9 with and without an electric field present. It is clear that without and electric field, the particle trajectories predominantly follow trapped J* contours to the wall. For the configuration used here, the magnetic field direction is such that ion trajectories precess around the J* contours in a counter-clockwise sense. With sufficient electric field to close off the trapped particle loss cone, the particle cloud becomes more isotropic and the associated losses are more diffusive in character.

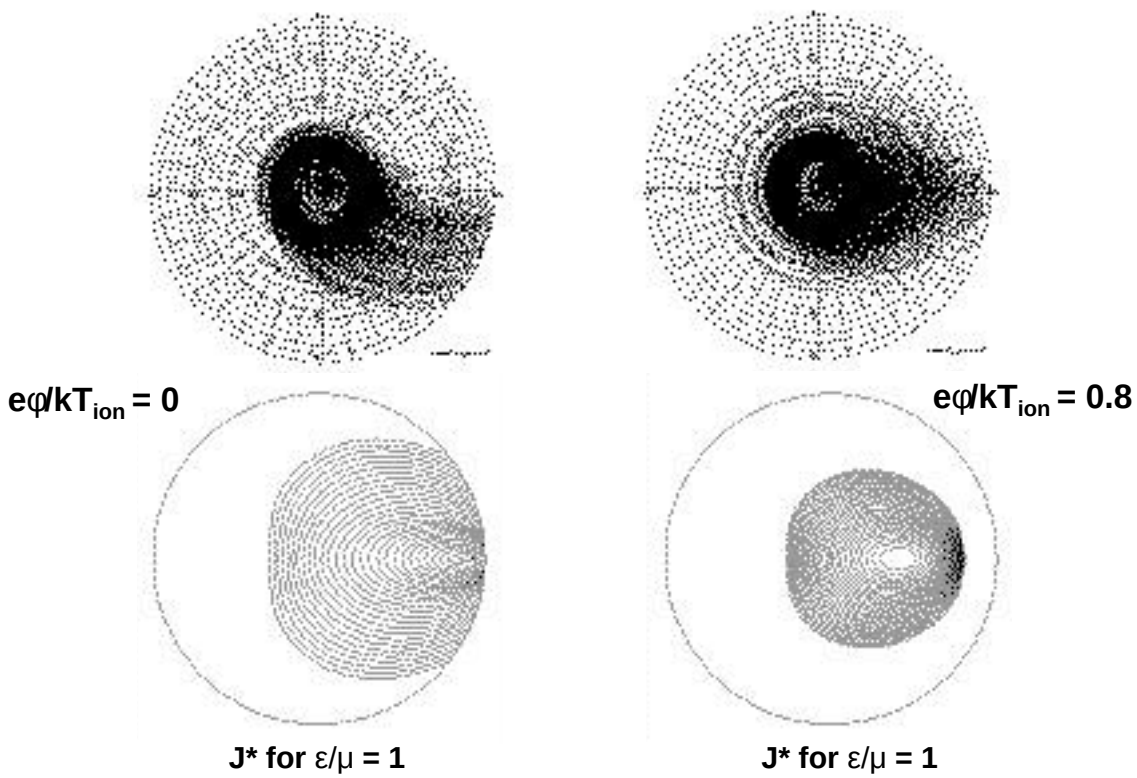

Figure 10 - Comparison of Monte Carlo particle trajectories with deeply trapped J* contours.

Although the present Monte Carlo model does not follow ions and electrons simultaneously, we have preliminary results from separate calculations comparing electron loss rates. Although the particle cloud plots for electrons also show direct losses above the midplane (since electrons precess in a clockwise direction) they are more smeared out due to the higher collisionality. The electron loss rates are also lower that those for ions, which tends to reinforce the direction chosen here for the electric field (pointing inward) in our ion transport studies.

IV. Magnetic Optimization

Recent stellarator design efforts[22,23,24] have focused much attention on magnetic coil optimization. This is motivated by a range of goals, such as the need to improve confinement, reduce bootstrap current, maintain a magnetic well, reduce ripple, etc. Our primary goal has been improved confinement of helically trapped particles within the constraints of preserving the aspect ratio, iota, and V″ well. Although ambipolar electric fields can generally close off the loss regions of thermal plasma species, some degree of magnetic optimization will be needed for the confinement of more energetic species, such as RF tails, beams, and, ultimately, alpha populations. Our results in the area of optimization of hybrid devices are very preliminary at this stage and will be discussed more fully in a subsequent paper.

Until recently, the dominant optimization techniques have generally focused on achieving some degree of symmetry in the structure of the magnetic field in Boozer coordinates since this is the context within which particle confinement is most readily influenced. Such symmetries are achieved through tailoring the shape of the magnetic flux surfaces which only influence particle confinement indirectly through their effect on the Boozer spectrum of |B|. Attaining these symmetries would then lead to an additional invariant which limits particle excursions away from flux surfaces. Most of the attention has been directed towards systems possessing either helical symmetry[22,24] (quasi-helical) or toroidal symmetry[23] (quasi-toroidal). Recently, an alternate approach, omnigeneity,[8,9] has also been suggested. This would attempt to improve confinement by directly reducing the bounce-averaged drift of particles away from flux surfaces. As suggested in Ref. 9, this approach is not as constraining as the quasi-symmetrization methods and can potentially open up wider regions of design space, especially at low aspect ratio. Results obtained in Refs. 8 and 9 indicate that omnigeneity can be reduced to the simple criterion of obtaining equal distances on a flux surface between the same values of |B| for the full range of |B| values on the surface.

In the following, we shall use the simpler criteria of centering B_{min} and B_{max} contours on flux contours, which can approximate omnigeneity[9] and is, in addition a prerequisite for attaining the equal distance criteria mentioned in Refs. 8 and 9. This should improve the confinement of the deeply trapped and transitionally trapped particles. The approach used is to vary the shape of the last closed flux surface iteratively, coupled with recalculation of the equilibrium and evaluation of the deviation of B_{min} and B_{max} from being constant upon some subset of flux surfaces. This loop is driven by a nonlinear least squares minimization algorithm (Levenberg-Marquardt) which attempts to search for the flux surface shape which minimizes the flux surface variation of B_{min} and B_{max}. Once the desired shape has been achieved, the final step (under development) in this process is then to work outward from the last closed flux surface to a coil configuration which is consistent with such a shape.

The above process has been applied to one of our vacuum field, zero current 8 field period configurations. In Figure 11 we plot B_{min} and B_{max} contours for the original and two of the optimized configurations.

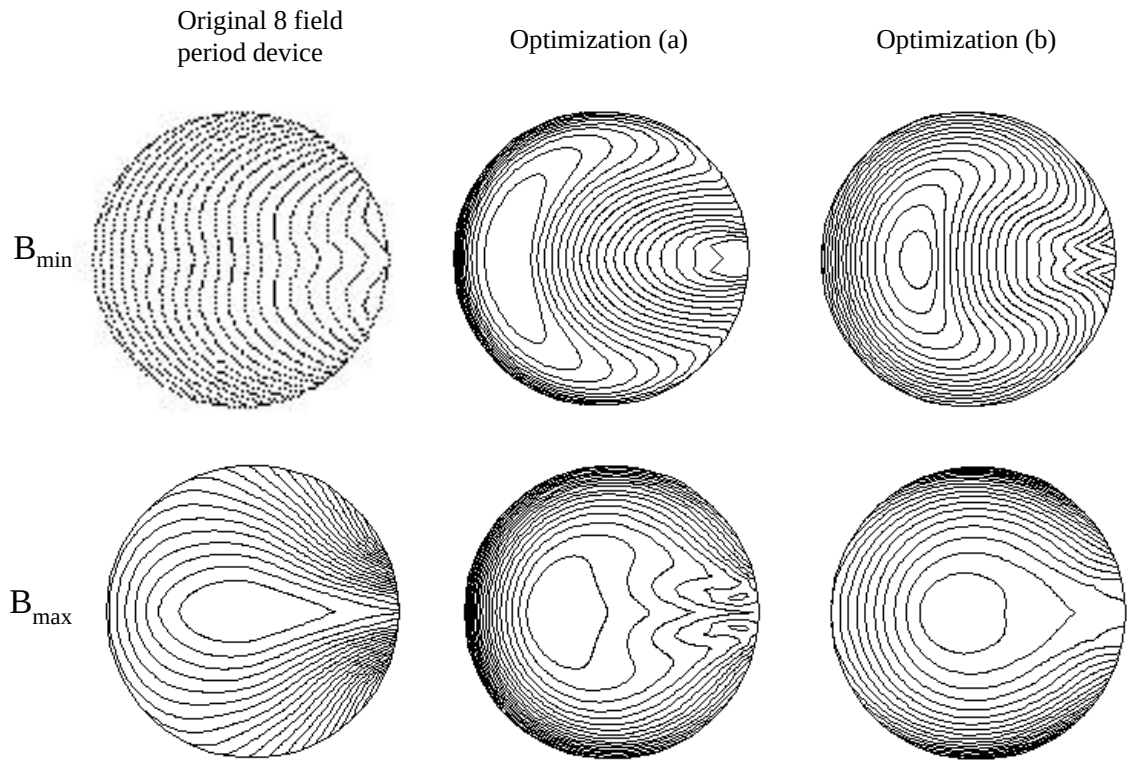

Figure 11 - B_{min} and B_{max} contours for the original un-optimized configuration and two optimized configurations.

These show the feasibility of this process for centering and closing such contours. They clearly are not yet functions of flux only (concentric circles), but the fact that there is, in particular, a significant volume of closed B_{min} contours in the optimized cases indicates that progress has been made in the confinement of deeply trapped orbits. In Figure 12 we plot the structure of |B| along a field line on the outermost flux surface for the 3 configurations.

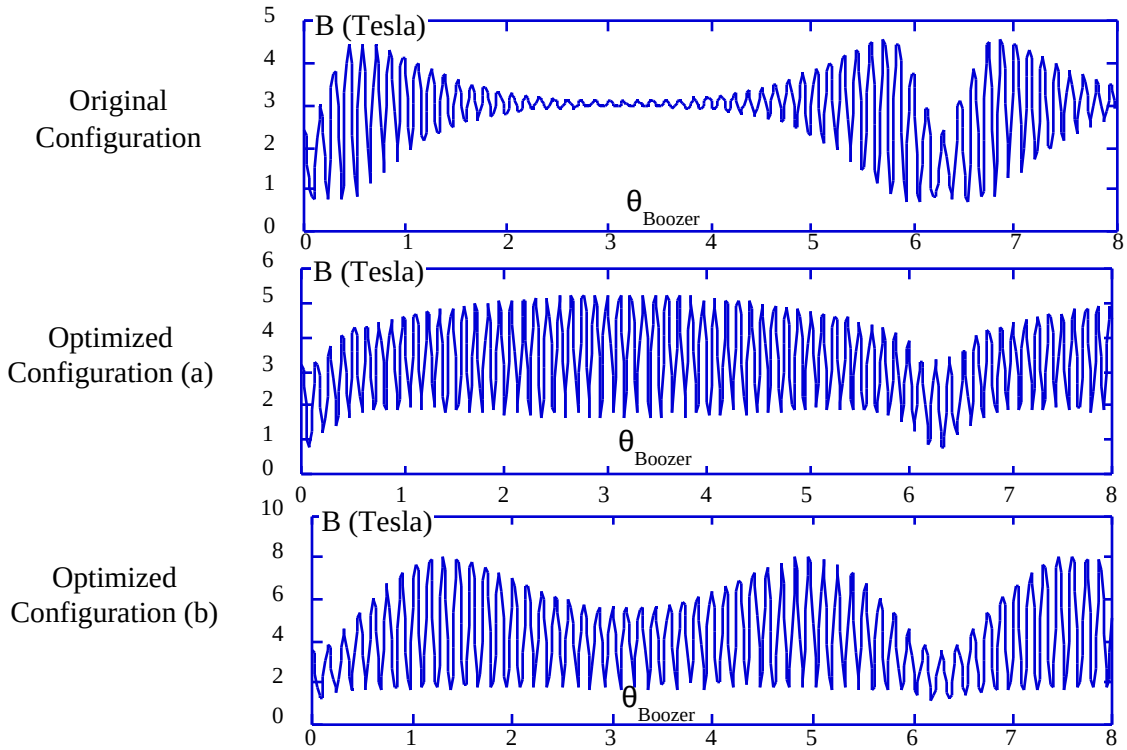

Figure 12 - Variation of |B| along a field line on the last closed outermost flux surface for un-optimized and optimized configurations.

The optimizations actually end up increasing the average ripple, although its distribution on the flux surface has changed. The beneficial effects on transport of redistributing ripple from the outside to the inside of a stellarator have been pointed out earlier.[25] The ideal state of B_{min} and B_{max} being only functions of flux would imply that the tops and bottoms of the oscillations of |B| in Figure 12 would be perfectly lined up. Although this has not yet been achieved here, the plots show that the optimization is moving the configuration in this direction. Finally, in Figure 13, we have plotted the loss rates obtained from our Monte Carlo model for the two optimized configurations relative to the original (un-optimized) configuration. This demonstrates the efficacy of the optimization procedure for lowering transport rates with about a factor of two reduction in loss rates in going from the original configuration to the second optimized system.

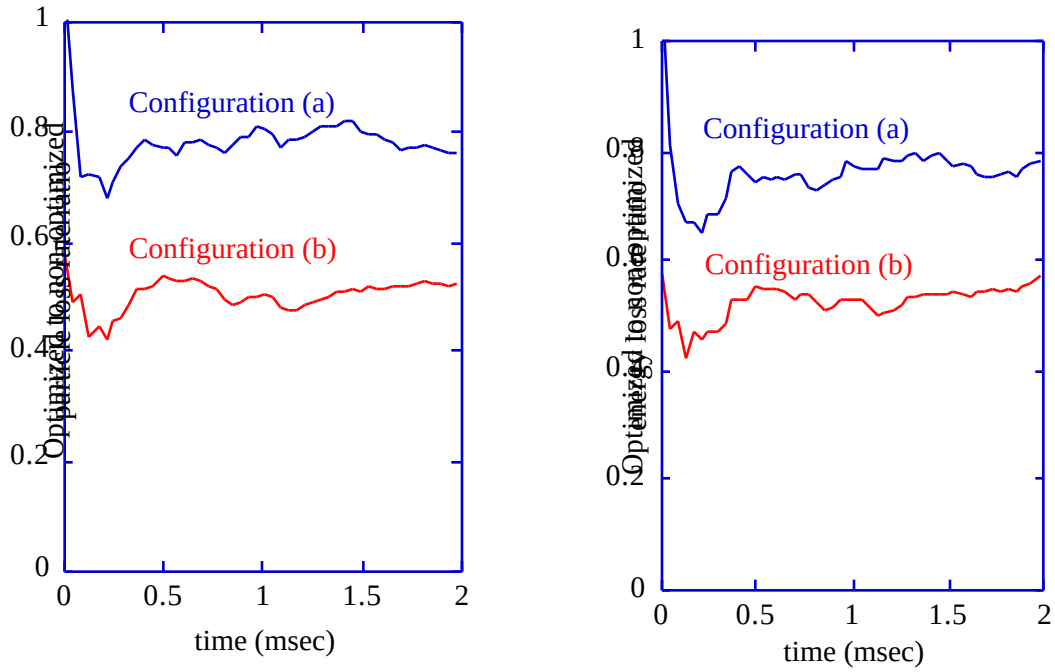

Figure 13 - Comparison of Monte Carlo particle and energy loss rates for the optimized configurations compared to the original configuration.

V. Conclusions

Transport and confinement are significant issues for low aspect ratio tokamak/stellarator hybrid configurations; these devices tend to have both large ripple and strong toroidal effects. We have applied a variety of tools towards assessing the confinement features of these devices: B_{min}, B_{max} contours, J* adiabatic invariant contours, guiding center orbit trajectories, and Monte Carlo simulations of transport. At low collisionality, a significant loss component comes from direct loss of the helically trapped orbits. Our results have indicated several directions to proceed for confinement improvement, including: control over the magnitude and profile of the electric field, adding toroidal plasma current, increasing magnetic field, and decreasing ripple. In addition, simplified criteria (i.e., closure and centering of B_{min}, B_{max} contours on flux surfaces) have been suggested for magnetic optimization and tested. Preliminary results based on these optimization targets indicate a factor of 2 reduction in global loss rates can be achieved. We would anticipate that further effort in this direction can lead to higher degrees of improvement.

Acknowledgments

This work has benefited from many useful discussions with Jim Rome, Jim Lyon, Ben Carreras, and Don Batchelor of Oak Ridge. This work has been supported by the U. S. Department of Energy Contract Number DE-AC05-960R22464 under contract with Oak Ridge National Laboratory managed by Lockheed-Martin Energy Research Corporation.

[1] P. E. Moroz, Phys. Rev.Lett., Vol. 77 (651) 1996.

[2] B. A. Carreras, V.E. Lynch, A. Ware, ORNL/TM-13252, August, 1996.

[3] P. E. Moroz, D. B. Batchelor, B. A. Carreras, S. P. Hirshman, D. K. Lee, V. E. Lynch, D. A. Spong, J. S. Tolliver, A. S. Ware, J. C. Whitson, Fusion Technology, Vol 30, No. 3, Part 2B (1347) 1996.
[4] D. W. Ross, et al., proceedings of US/Japan JIFT Workshop, Columbia University, Oct. 14, 1996.
[5] D. B. Batchelor, et al., proceedings of US/Japan JIFT Workshop, Columbia University, Oct. 14, 1996.
[6] J. D. Hanson, et al., proceedings of US/Japan JIFT Workshop, Columbia University, Oct. 14, 1996.
[7] D. A. Garren, A. H. Boozer, Phys. Fluids B3, 2822 (1991).
[8] A. A. Skovoroda, V. D. Shafranov, Plasma Physics Reports, Vol. 21 (937) 1995.
[9] J. R. Cary, S. G. Shasharina, Univ. of Colorado report CIPS-001, 1996; also, see proceedings of US/Japan JIFT Workshop, Columbia University, Oct. 14, 1996.
[10] S. P. Hirshman, J. C. Whitson, Phys. Fluids Vol. 26 (3553) 1983.
[11] A. H. Boozer, Phys. Fluids, Vol. 23 (904) 1980.
[12] J. R. Cary, C. L. Hedrick, J. S. Tolliver, Phys. Fluids Vol. 31 (1586) 1988.
[13] J. A. Rome, Nuclear Fusion. Vol 35 (195) 1995.
[14] J. R. Cary, et al., Phys. Fluids Vol. 31 (1586) 1988.
[15] S. V. Bulanov, S. G. Shasharina, Nuclear Fusion, Vol. 32 (1531) 1992.
[16] R. H. Fowler, J. A. Rome, J. F. Lyon, Phys. Fluids, Vol. 28 (338) 1995.
[17] A. H. Boozer, G. Kuo-Petravic, Phys. Fluids, Vol. 24 (851) 1981.
[18] P. R. Garabedian, M. Taylor, Nuclear Fusion, Vol. 32 (265) 1992; also, see N. M. Kuhl, Journal of Computational Physics, Vol 129 (170) 1996.
[19] M. Sasinowski, A. H. Boozer, Phys. Plasmas, Vol. 2 (610) 1995.
[20] W. I. Van Rij, S. P. Hirshman, Phys. Fluids, B1 (563) 1989.
[21] J. F. Lyon, et al., Fusion Technology, Vol. 10 (179) 1986.
[22] J. Nührenberg, R. Zille, Physics Letters A, 129 (113) 1988.
[23] P. Garabedian, Phys. Plasmas, Vol. 3 (2483) 1966.
[24] D. T. Anderson, P. R. Garabedian, Nuclear Fusion, Vol. 34 (881) 1994.
[25] H. E. Mynick, T. K. Chu, A. H. Boozer, Phys. Rev. Lett., Vol. 48 (322) 1982.